SARS-CoV-2 protein ORF3a is pathogenic in *Drosophila* and causes phenotypes associated with COVID-19 post-viral syndrome

Shuo Yang[1], Meijie Tian[2], and Aaron N. Johnson[1,3]

[1]Department of Developmental Biology
Washington University School of Medicine
St. Louis, MO 63110

[2]Genetics Branch, Oncogenomics Section
National Cancer Institute, NIH
Bethesda, MD 20892

[3]Author for correspondence: anjohnson@wustl.edu

Highlights

SARS-CoV-2 ORF3a is pathogenic in the nervous system.

ORF3a induces cell death, inflammation, and lysosome dysfunction.

Chloroquine protects against ORF3a induced CNS distress and lysosome dysfunction.

Summary

The Coronavirus Disease 2019 (COVID-19) pandemic has caused millions of deaths and will continue to exact incalculable tolls worldwide. While great strides have been made toward understanding and combating the mechanisms of Severe Acute Respiratory Syndrome Coronavirus-2 (SARS-CoV-2) infection, relatively little is known about the individual SARS-CoV-2 proteins that contribute to pathogenicity during infection and that cause neurological sequela after viral clearance. We used *Drosophila* to develop an *in vivo* model that characterizes mechanisms of SARS-CoV-2 pathogenicity, and found ORF3a adversely affects longevity and motor function by inducing apoptosis and inflammation in the nervous system. Chloroquine alleviated ORF3a induced phenotypes in the CNS, arguing our *Drosophila* model is amenable to high throughput drug screening. Our work provides novel insights into the pathogenic nature of SARS-CoV-2 in the nervous system that can be used to develop new treatment strategies for post-viral syndrome.

Main Text

SARS-CoV-2 is the causative agent of the ongoing COVID-19 pandemic, which has resulted in more than 1.5 million deaths worldwide (JHU, 2020). To stem the spread of SARS-CoV-2 and control the COVID-19 pandemic, SARS-CoV-2 research has primarily focused on understanding the mechanisms of viral infection and transmission. For example, ACE2 encodes a SARS-CoV-2 receptor, and humanized ACE2 transgenic mice have been developed to investigate the mechanisms of SARS-CoV-2 infection *in vivo* (Jiang et al., 2020; Kim et al., 2020; Sun et al., 2020). In contrast, relatively little is known about how specific SARS-CoV-2 proteins induce pathogenesis (Kumar et al., 2020). The high COVID-19 mortality rate suggests that proteins encoded by the SARS-CoV-2 genome are unusually virulent. After the active SARS-CoV-2 infection is cleared, or no longer detectable, a majority of recovering patients will experience post viral syndrome with indications that include neuropsychiatric symptoms and extreme fatigue lasting for several months (Mooney et al., 2020; Townsend and Dyer, 2020). As recently developed vaccines begin to control the COVID-19 pandemic, it will be critically important to identify the mechanisms by which SARS-CoV-2 proteins cause pathogenesis in order to develop treatments that mitigate the adverse affects associated with the sequela of infection.

The SARS-Cov-2 genome encodes 11 genes with 14 open reading frames (ORFs), that produce a total of 29 proteins including 16 nonstructural proteins (NSP1-NSP16), 4 structural proteins (spike protein [S)], membrane protein [M], nucleocapsid protein [N], envelope protein [E]), and 9 accessory proteins (ORF3a, ORF3b, ORF6, ORF7a, ORF7b, ORF8, ORF9b, ORF9c and ORF10)(Gordon et al., 2020). The ORF3a protein is unique to coronaviruses and has been characterized in SARS-CoV, which caused the severe acute respiratory syndrome (SARS) outbreak in 2003. SARS-CoV ORF3a triggers a pathogenic inflammatory reaction through its interaction with TRAF3 that drives IL-1/IL-18 maturation and ultimately causes severe lung damage through cell pyroptosis and apoptosis (Siu et al., 2019). Moreover, SARS-CoV ORF3a induces vesicle formation and golgi fragmentation, which are prominent features observed in patient samples (Freundt et al., 2010). SARS-CoV-2 ORF3a might also be pathogenic. *In vitro* studies show SARS-CoV-2 ORF3a induces caspase-dependent apoptosis (Ren et al., 2020), while *in silico* studies argue that the ORF3a mutation rate directly correlates with SARS-CoV-2 mortality rates after infection (Majumdar and Niyogi, 2020). In addition, SARS-CoV-2 ORF3a facilitates virus replication by high jacking the autophagy machinery; despite 72.36% amino acid identity between the ORF3a proteins (Fig. S1A), SARS-CoV ORF3a does not promote viral replication (Qu et al., 2020). Although these studies suggest that SARS-CoV-2 ORF3a has unique pathogenic functions that contribute to the relatively high COVID-19 mortality rate, an *in vivo* model has yet to be developed that specifically interrogates the mechanisms of SARS-CoV-2 ORF3a pathogenicity.

To date, clinical treatments are not available that alleviate SARS-CoV-2 post viral syndrome. Identifying drugs that treat COVID-19 remains an urgent need, but the low availability of hACE2 transgenic mice and the requirement for P3-level infrastructure to handle SARS-CoV-2 viruses prevents a vast majority of laboratories from conducting COVID-19 research. An alternative strategy is to develop *in vivo* models of SARS-CoV-2 pathogenicity in which candidate drugs targeting specific viral proteins can be tested for protection against pathogenic outcomes. Promising therapeutic strategies would include compounds that block hyperinflammation and apoptosis induced by pathogenic viral proteins (Freeman and Swartz, 2020; van den Berg and Te Velde, 2020; Yap et al., 2020).

The powerful genetic tools in *Drosophila* have been used to identify essential mechanisms that

53 underlie viral infections (Hao et al., 2008; Hughes et al., 2012; Yang et al., 2018), and that contribute to
54 viral pathogenicity (Adamson et al., 2011; Chan et al., 2009; Harsh et al., 2020). In addition, the short
55 lifespan with easy-to-score visible phenotypes has made the fruit fly a productive *in vivo* drug screening
56 platform (Chang et al., 2008; Dar et al., 2012; Su, 2019; Willoughby et al., 2013). Here, we report the
57 development and characterization of an *in vivo Drosophila* model that assays SARS-CoV-2 proteins for
58 tissue-specific pathogenicity and that can successfully identify drug candidates that mitigate pathogenic
59 SARS-CoV-2 proteins.

60 We constructed a transgenic fly that placed ORF3a under UAS control. SARS-CoV-2 infection
61 shows a strong tissue preference, most notably affecting the respiratory system, due to the usual route
62 of infection and the relative abundance of ACE2 among tissues (Hikmet et al., 2020; Puelles et al., 2020).
63 To understand if SARS-CoV-2 pathogenicity can also be tissue-specific, we used the bipartite
64 GAL4/UAS system to express ORF3a in the central nervous system (CNS; *elav.Gal4*), in photoreceptors
65 (*GMR.Gal4*), and in striated and smooth muscle (*Mef2.Gal4*). Each Gal4 driver robustly induced ORF3a
66 expression (Fig. 1A, S1B,C), but appreciable phenotypes were only observed in flies that expressed
67 ORF3a in the nervous system. ORF3a expression in the CNS significantly reduced lifespan (control
68 median survival>14d, n=60; *elav>ORF3a*=5.0d, n=65; Fig 1B), impaired motor function in longitudinal
69 climbing assays (average performance *elav>ORF3a* =1.9% of control, n>60 per genotype; Fig. 1C, S1D),
70 and induced pronounced abdominal swelling (>90% individuals, n=65, Fig. S1E). Fewer *elav>ORF3a*
71 adult flies eclosed than expected (49.5% of expected, n=188; Fig. 1D), suggesting ORF3a caused
72 partial lethality during larval stages. In addition, flies that expressed ORF3a in photoreceptors showed a
73 rough eye phenotype, which is consistent with defects in ommatidia patterning and apoptosis (100%
74 affected, n>100; Fig. 1E). Surprisingly, ORF3a expression in muscle did not significantly affect longevity,
75 motor function, or muscle patterning (Fig. 1F, S1F). Consistent with these results, >35% of COVID-19
76 patients showed neurological symptoms whereas <10% of patients showed musculoskeletal
77 complications (Mao et al., 2020). These studies argue that ORF3a is pathogenic in only a subset of
78 tissues, and that the CNS is particularly sensitive to ORF3a expression.

79 After establishing a primary infection in the respiratory system, SARS-CoV and SARS-CoV-2 can

80 pass the blood-brain barrier and efficiently infect the CNS (Glass et al., 2004; Meinhardt et al., 2020;
81 Puelles et al., 2020; Zheng et al., 2020), and SARS-CoV-2 has been associated with a host of
82 neurological symptoms including impaired consciousness, stroke, concentration problems, memory loss,
83 dizziness and insomnia (Mao et al., 2020). Reduced lifespan and impaired motor function in
84 *elav>ORF3a* flies are phenotypes indicative of neurodegeneration (Moore et al., 2018), so we assessed
85 apoptosis in the adult brain, and found that ORF3a induced Caspase-3 cleavage (Fig. 1G).
86 Neuroinflammation is often seen in COVID-19 patients, possibly via damage-associated molecular
87 patterns (DAMPs) induced TLR4-MyD88 signaling activation (Meinhardt et al., 2020; Ren et al., 2020;
88 Zhou et al., 2020). In *Drosophila*, non-infectious sterile inflammation can be initiated when necrotic cells
89 release DAMPs that in turn activate immunoinflammatory pathways, including the Toll and IMD
90 pathways (Kosakamoto et al., 2020; Obata et al., 2014). We hypothesized that ORF3a elicits a sterile
91 inflammatory response, and found that expressing ORF3a in the CNS induced Toll pathway reporter
92 expression (fold change vs control, *Drs*=10.2; Fig. 1H) and IMD reporter expression (*dipt*=28.8,
93 *attA*=55.9)(Yang et al., 2019). We also assayed *eiger* expression, which is a marker for Jun kinase
94 (JNK)-mediated inflammation and apoptosis (Li et al., 2019), but *eiger* expression was not significantly
95 changed in *elav>ORF3a* flies (Fig. 1I). These data demonstrate that ORF3a expression alone is
96 sufficient to cause apoptosis, neuroinflammation, and neurotropism, and suggest ORF3a is a major
97 virulence factor of SARS-CoV-2. Thus our ORF3a transgenic fly model recapitulates hallmarks of
98 SARS-CoV-2 infection reported in patients and cell culture systems.

99 We next wanted to understand if our ORF3a model could be used to identify COVID-19 treatments.
100 In Vero cells, lysosome deacidification is essential for virus egress, and ORF3a localized to lysosomes
101 and caused lysosome deacidification (Ghosh et al., 2020). Toxic stress also caused lysosome
102 deacidification in U2OS cells, and chloroquine phosphate (CQ) blocked chemically induced
103 deacidification (Mauthe et al., 2018). Although CQ did not consistently prevent SARS-CoV-2 infections
104 in clinical trials, the ORF3a lysosome studies suggested that CQ could prevent ORF3a-induced tropism.
105 To understand if our fly model could respond to COVID-19 treatments, we tested the efficacy of CQ in
106 mitigating ORF3a phenotypes. CQ treated *elav>ORF3a* flies showed significantly longer lifespans

107 (*elav>ORF3a* median survival=6d, n=121; *elav>ORF3a*+CQ=14d, n=79; Fig 2A), and improved motor
108 function compared to untreated controls (average performance *elav>ORF3a*=1.3% of control;
109 *elav>ORF3a*+CQ=9.8% of control; n>60 per genotype; Fig 2B). In addition, more CQ treated
110 *elav>ORF3a* adult flies eclosed than untreated controls (treated=72.4% of expected, n=174;
111 untreated=49.5%; Fig. 2C), suggesting CQ can suppress ORF3a induced larval lethality. These proof of
112 principle studies largely validate our ORF3a *Drosophila* model as an efficient COVID-19 drug-screening
113 platform.

114 At the molecular level, CQ treated *elav>ORF3a* flies showed reduced cleaved-caspase-3 levels
115 (untreated FC=2.3; treated FC=1.3; Figure 2D), and reduced Toll pathway activity (*Drs;* FC=0.43 vs
116 untreated; Fig. 2E) compared to untreated controls. However, IMD pathway reporters did not respond to
117 CQ treatment (*dipt*=0.75, *attA*=0.89). One mechanism that might explain CQ specificity is that the Toll
118 pathway is a more direct target of necrotic derived DAMPs, while the IMD pathway is not (Kosakamoto
119 et al., 2020). A second mechanism of action for CQ could involve ORF3a-induced lysosome dysfunction.
120 LysoTracker is a vital dye that accumulates in acidic organelles and is often used as a marker for
121 lysosome function (Sanman et al., 2016). Similar to Vero cells, ORF3a promoted lysosome
122 deacidification in HeLa cells (Fig. 2G,H). Strikingly, we found CQ treatment efficiently blunted ORF3a
123 induced deacidification (Fig. 2G,H). While CQ showed no effect on inpatient survival (Geleris et al.,
124 2020), our results argue CQ prevents apoptosis and lysosome dysfunction in ORF3a-expressing cells,
125 and suggest CQ could ameliorate symptoms associated with SARS-CoV-2 post viral syndrome in
126 recovering patients (Fig. 2I).

127 The sequela of SARS-CoV-2 infection includes extensive neurological complications such as
128 problems with concentration, memory loss, anxiety and depression (Halpin et al., 2020). Since the
129 duration and severity of persistent symptoms among COVID-19 survivors is continuing to emerge,
130 understanding and treating COVID-19 post viral syndrome will be a high healthcare priority over the next
131 several years. Time course studies of SARS-CoV-2 infection, replication, and clearance have yet to be
132 reported in detail, but infection parameters have been defined for the closely related SARS-CoV in mice
133 (Glass et al., 2004). SARS-CoV was detectable in the lungs for up to 9 days after an initial nasal

134 inoculation, and then spread to the CNS where the virus was detectable for an additional 6 days (Glass
135 et al., 2004). Interestingly, after infectious SARS-CoV, SARS-CoV-2, and the coronavirus Middle East
136 Respiratory Syndrome (MERS)-CoV has been cleared, viral RNA continues to be detectable in many
137 tissues (Glass et al., 2004; Sia et al., 2020; Widagdo et al., 2019).

138 Our study revealed ORF3a expression in the nervous system alone can induce cell death and
139 neuroinflammation, suggesting ORF3a is the major virulence factor contributing to SARS-CoV-2
140 induced neurotropism (Figs. 1B,C). In addition, the gold standard PCR-based SARS-CoV-2 test can
141 only assess viral load in the respiratory system. After SARS-CoV-2 is cleared from the respiratory
142 system, and a patient tests negative, SARS-CoV-2 may continue to replicate in the CNS (Fig. 2J). The
143 residual ORF3a may continue to trigger neurological complications associated with post viral syndrome
144 in recovering patients, suggesting continued medical treatments are in fact required for full recovery
145 after a 'negative' PCR-based SARS-CoV-2 test.

146 In summary, our results warrant further studies of SARS-CoV-2 pathogenic mechanisms as a
147 means to treat COVID-19 post viral syndrome and identify ORF3a as a high priority target that is
148 amenable to drug treatment (Fig. 2A,B). A future drug screen with ORF3a transgenic flies will likely
149 reveal post-viral syndrome treatments beyond CQ.

Acknowledgments

We thank Jennifer McAdow, Yingqiu Du, and Tiffany Ou for technical support throughout the project. We also thank Mayssa Mokalled for the relentless encouragement. ANJ was supported by NIH R01AR070299.

Author Contributions

Conceptualization, S.Y., M.T. and ANJ.; Methodology and Validation, S.Y.; Formal Analysis, S.Y., M.T., and ANJ.; Investigation, S.Y. and M.T.; Resources, ANJ.; Writing-Original Draft, S.Y., M.T. and ANJ.; Supervision, ANJ.; Funding Acquisition, ANJ.

Declaration Of Interests

The authors declare no competing interests.

References

150 Adamson, A.L., Chohan, K., Swenson, J., and LaJeunesse, D. (2011). A Drosophila model for genetic analysis of
151 influenza viral/host interactions. Genetics *189*, 495-506.
152 Chan, C.M., Tsoi, H., Chan, W.M., Zhai, S., Wong, C.O., Yao, X., Chan, W.Y., Tsui, S.K., and Chan, H.Y. (2009). The ion
153 channel activity of the SARS-coronavirus 3a protein is linked to its pro-apoptotic function. Int J Biochem Cell Biol *41*,
154 2232-2239.
155 Chang, S., Bray, S.M., Li, Z., Zarnescu, D.C., He, C., Jin, P., and Warren, S.T. (2008). Identification of small molecules
156 rescuing fragile X syndrome phenotypes in Drosophila. Nat Chem Biol *4*, 256-263.
157 Dar, A.C., Das, T.K., Shokat, K.M., and Cagan, R.L. (2012). Chemical genetic discovery of targets and anti-targets for
158 cancer polypharmacology. Nature *486*, 80-84.
159 Freeman, T.L., and Swartz, T.H. (2020). Targeting the NLRP3 Inflammasome in Severe COVID-19. Front Immunol *11*,
160 1518.
161 Freundt, E.C., Yu, L., Goldsmith, C.S., Welsh, S., Cheng, A., Yount, B., Liu, W., Frieman, M.B., Buchholz, U.J., Screaton, G.R.*,*
162 *et al.* (2010). The open reading frame 3a protein of severe acute respiratory syndrome-associated coronavirus
163 promotes membrane rearrangement and cell death. J Virol *84*, 1097-1109.
164 Geleris, J., Sun, Y., Platt, J., Zucker, J., Baldwin, M., Hripcsak, G., Labella, A., Manson, D.K., Kubin, C., Barr, R.G.*, et al.*
165 (2020). Observational Study of Hydroxychloroquine in Hospitalized Patients with Covid-19. N Engl J Med *382*,
166 2411-2418.
167 Ghosh, S., Dellibovi-Ragheb, T.A., Kerviel, A., Pak, E., Qiu, Q., Fisher, M., Takvorian, P.M., Bleck, C., Hsu, V.W., Fehr, A.R.*,*
168 *et al.* (2020). beta-Coronaviruses Use Lysosomes for Egress Instead of the Biosynthetic Secretory Pathway. Cell.
169 Glass, W.G., Subbarao, K., Murphy, B., and Murphy, P.M. (2004). Mechanisms of host defense following severe acute
170 respiratory syndrome-coronavirus (SARS-CoV) pulmonary infection of mice. J Immunol *173*, 4030-4039.
171 Gordon, D.E., Jang, G.M., Bouhaddou, M., Xu, J., Obernier, K., White, K.M., O'Meara, M.J., Rezelj, V.V., Guo, J.Z., Swaney,
172 D.L.*, et al.* (2020). A SARS-CoV-2 protein interaction map reveals targets for drug repurposing. Nature *583*, 459-468.
173 Halpin, S.J., McIvor, C., Whyatt, G., Adams, A., Harvey, O., McLean, L., Walshaw, C., Kemp, S., Corrado, J., Singh, R.*, et al.*
174 (2020). Postdischarge symptoms and rehabilitation needs in survivors of COVID-19 infection: A cross-sectional
175 evaluation. Journal of Medical Virology *n/a*.
176 Hao, L., Sakurai, A., Watanabe, T., Sorensen, E., Nidom, C.A., Newton, M.A., Ahlquist, P., and Kawaoka, Y. (2008).
177 Drosophila RNAi screen identifies host genes important for influenza virus replication. Nature *454*, 890-893.
178 Harsh, S., Fu, Y., Kenney, E., Han, Z., and Eleftherianos, I. (2020). Zika virus non-structural protein NS4A restricts eye
179 growth in Drosophila through regulation of JAK/STAT signaling. Dis Model Mech *13*.
180 Hikmet, F., Mear, L., Edvinsson, A., Micke, P., Uhlen, M., and Lindskog, C. (2020). The protein expression profile of ACE2
181 in human tissues. Mol Syst Biol *16*, e9610.
182 Hughes, T.T., Allen, A.L., Bardin, J.E., Christian, M.N., Daimon, K., Dozier, K.D., Hansen, C.L., Holcomb, L.M., and
183 Ahlander, J. (2012). Drosophila as a genetic model for studying pathogenic human viruses. Virology *423*, 1-5.
184 JHU (2020). Johns Hopkins Coronavirus Resource Center.
185 Jiang, R.D., Liu, M.Q., Chen, Y., Shan, C., Zhou, Y.W., Shen, X.R., Li, Q., Zhang, L., Zhu, Y., Si, H.R.*, et al.* (2020).
186 Pathogenesis of SARS-CoV-2 in Transgenic Mice Expressing Human Angiotensin-Converting Enzyme 2. Cell *182*,
187 50-58 e58.
188 Kim, Y.I., Kim, S.G., Kim, S.M., Kim, E.H., Park, S.J., Yu, K.M., Chang, J.H., Kim, E.J., Lee, S., Casel, M.A.B.*, et al.* (2020).
189 Infection and Rapid Transmission of SARS-CoV-2 in Ferrets. Cell Host Microbe *27*, 704-709 e702.

190 Kosakamoto, H., Yamauchi, T., Akuzawa-Tokita, Y., Nishimura, K., Soga, T., Murakami, T., Mori, H., Yamamoto, K.,
191 Miyazaki, R., Koto, A.*, et al.* (2020). Local Necrotic Cells Trigger Systemic Immune Activation via Gut Microbiome
192 Dysbiosis in Drosophila. Cell Rep *32*, 107938.
193 Kumar, A., Prasoon, P., Kumari, C., Pareek, V., Faiq, M.A., Narayan, R.K., Kulandhasamy, M., and Kant, K. (2020).
194 SARS-CoV-2-specific virulence factors in COVID-19. J Med Virol.
195 Li, M., Sun, S., Priest, J., Bi, X., and Fan, Y. (2019). Characterization of TNF-induced cell death in Drosophila reveals
196 caspase- and JNK-dependent necrosis and its role in tumor suppression. Cell death & disease *10*, 613.
197 Majumdar, P., and Niyogi, S. (2020). ORF3a mutation associated higher mortality rate in SARS-CoV-2 infection.
198 Epidemiol Infect, 1-16.
199 Mao, L., Jin, H., Wang, M., Hu, Y., Chen, S., He, Q., Chang, J., Hong, C., Zhou, Y., Wang, D.*, et al.* (2020). Neurologic
200 Manifestations of Hospitalized Patients With Coronavirus Disease 2019 in Wuhan, China. JAMA Neurol *77*, 683-690.
201 Mauthe, M., Orhon, I., Rocchi, C., Zhou, X., Luhr, M., Hijlkema, K.J., Coppes, R.P., Engedal, N., Mari, M., and Reggiori, F.
202 (2018). Chloroquine inhibits autophagic flux by decreasing autophagosome-lysosome fusion. Autophagy *14*,
203 1435-1455.
204 Meinhardt, J., Radke, J., Dittmayer, C., Franz, J., Thomas, C., Mothes, R., Laue, M., Schneider, J., Brünink, S., Greuel, S.*, et*
205 *al.* (2020). Olfactory transmucosal SARS-CoV-2 invasion as a port of central nervous system entry in individuals with
206 COVID-19. Nature neuroscience.
207 Mooney, A., Gaffney, F., Jones, K., Dunne, J., O'Connor, L., Leavy, D., O'Brien, K., Dowds, J., Sugrue, J.A., Hopkins, D.*, et*
208 *al.* (2020). PLoS One.
209 Moore, B.D., Martin, J., de Mena, L., Sanchez, J., Cruz, P.E., Ceballos-Diaz, C., Ladd, T.B., Ran, Y., Levites, Y., Kukar, T.L.,
210 *et al.* (2018). Short Abeta peptides attenuate Abeta42 toxicity in vivo. J Exp Med *215*, 283-301.
211 Obata, F., Kuranaga, E., Tomioka, K., Ming, M., Takeishi, A., Chen, C.H., Soga, T., and Miura, M. (2014). Necrosis-driven
212 systemic immune response alters SAM metabolism through the FOXO-GNMT axis. Cell Rep *7*, 821-833.
213 Puelles, V.G., Lutgehetmann, M., Lindenmeyer, M.T., Sperhake, J.P., Wong, M.N., Allweiss, L., Chilla, S., Heinemann, A.,
214 Wanner, N., Liu, S.*, et al.* (2020). Multiorgan and Renal Tropism of SARS-CoV-2. N Engl J Med *383*, 590-592.
215 Qu, Y., Wang, X., Zhu, Y., Wang, Y., Yang, X., Hu, G., Liu, C., Li, J., Ren, S., Xiao, Z.*, et al.* (2020). ORF3a
216 mediated-incomplete autophagy facilitates SARS-CoV-2 replication. bioRxiv, 2020.2011.2012.380709.
217 Ren, Y., Shu, T., Wu, D., Mu, J., Wang, C., Huang, M., Han, Y., Zhang, X.Y., Zhou, W., Qiu, Y.*, et al.* (2020). The ORF3a
218 protein of SARS-CoV-2 induces apoptosis in cells. Cell Mol Immunol *17*, 881-883.
219 Sanman, L.E., van der Linden, W.A., Verdoes, M., and Bogyo, M. (2016). Bifunctional Probes of Cathepsin Protease
220 Activity and pH Reveal Alterations in Endolysosomal pH during Bacterial Infection. Cell chemical biology *23*, 793-804.
221 Sia, S.F., Yan, L.M., Chin, A.W.H., Fung, K., Choy, K.T., Wong, A.Y.L., Kaewpreedee, P., Perera, R., Poon, L.L.M., Nicholls,
222 J.M.*, et al.* (2020). Pathogenesis and transmission of SARS-CoV-2 in golden hamsters. *583*, 834-838.
223 Siu, K.L., Yuen, K.S., Castano-Rodriguez, C., Ye, Z.W., Yeung, M.L., Fung, S.Y., Yuan, S., Chan, C.P., Yuen, K.Y., Enjuanes,
224 L.*, et al.* (2019). Severe acute respiratory syndrome coronavirus ORF3a protein activates the NLRP3 inflammasome by
225 promoting TRAF3-dependent ubiquitination of ASC. FASEB J *33*, 8865-8877.
226 Su, T.T. (2019). Drug screening in Drosophila; why, when, and when not? Wiley Interdiscip Rev Dev Biol *8*, e346.
227 Sun, S.H., Chen, Q., Gu, H.J., Yang, G., Wang, Y.X., Huang, X.Y., Liu, S.S., Zhang, N.N., Li, X.F., Xiong, R.*, et al.* (2020). A
228 Mouse Model of SARS-CoV-2 Infection and Pathogenesis. Cell Host Microbe *28*, 124-133 e124.
229 Townsend, L., and Dyer, A.H. (2020). Persistent fatigue following SARS-CoV-2 infection is common and independent
230 of severity of initial infection. *15*, e0240784.

van den Berg, D.F., and Te Velde, A.A. (2020). Severe COVID-19: NLRP3 Inflammasome Dysregulated. Front Immunol *11*, 1580.

Widagdo, W., Sooksawasdi Na Ayudhya, S., Hundie, G.B., and Haagmans, B.L. (2019). Host Determinants of MERS-CoV Transmission and Pathogenesis. Viruses *11*.

Willoughby, L.F., Schlosser, T., Manning, S.A., Parisot, J.P., Street, I.P., Richardson, H.E., Humbert, P.O., and Brumby, A.M. (2013). An in vivo large-scale chemical screening platform using Drosophila for anti-cancer drug discovery. Dis Model Mech *6*, 521-529.

Yang, S., Yu, J., Fan, Z., Gong, S.T., Tang, H., and Pan, L. (2018). Bub1 Facilitates Virus Entry through Endocytosis in a Model of Drosophila Pathogenesis. J Virol *92*.

Yang, S., Zhao, Y., Yu, J., Fan, Z., Gong, S.T., Tang, H., and Pan, L. (2019). Sugar Alcohols of Polyol Pathway Serve as Alarmins to Mediate Local-Systemic Innate Immune Communication in Drosophila. Cell Host Microbe *26*, 240-251 e248.

Yap, J.K.Y., Moriyama, M., and Iwasaki, A. (2020). Inflammasomes and Pyroptosis as Therapeutic Targets for COVID-19. J Immunol *205*, 307-312.

Zheng, J., Wong, L.R., Li, K., Verma, A.K., Ortiz, M.E., Wohlford-Lenane, C., Leidinger, M.R., Knudson, C.M., Meyerholz, D.K., McCray, P.B., Jr.*, et al.* (2020). COVID-19 treatments and pathogenesis including anosmia in K18-hACE2 mice.

Zhou, T., Su, T.T., Mudianto, T., and Wang, J. (2020). Immune asynchrony in COVID-19 pathogenesis and potential immunotherapies. J Exp Med *217*.

Materials and methods

Drosophila genetics

249 The Gal4 stocks used to express SARS-CoV-2 ORF3a in brain, eye, and muscle included
250 P{GAL4-elav.L} (Bloomington Stock Center, 8760), P{GAL4-ninaE.GMR} (Bloomington Stock Center,
251 1104), and P{Mef2-GAL4.247} (Bloomington Stock Center, 50742). Flies were maintained on standard
252 "Bloomington recipe" media, and cultured at 25 °C under a normal light/dark cycle, unless otherwise
253 noted.

Transgenic Flies

254 *UAS-SARS-CoV-2-ORF3a* transgenic flies were generated by PCR-mediated subcloning of the
255 SARS-CoV-2-ORF3a coding sequence (pDONR207 SARS-CoV-2 ORF3A, #141271, Addgene) into
256 pUASt-Attb (EcoRI/XbaI). ORF3a was amplified with Takara PrimerSTAR PCR enzyme (R050B, Takara)
257 using the following primers:
258 ORF3a-CDS-Forward- CGGAATTCATGGACCTGTTCATGAGAATCTT
259 ORF3a-CDS-Rerverse-GCTCTAGATTACAGTGGCACGGAGGTG
260 Plasmid DNA was injected and targeted to a C31 integration site at 22A2 (Bloomington Stock 24481,
261 Rainbow Transgenic Flies); stable insertions were identified by standard methods.

Immunohistochemistry and imaging

262 Antibodies used include anti-SARS-CoV-2-ORF3a (1:200, 101AP, FabGennix International Inc),
263 anti-Tropomyosin (1:600, MAC141, Abcam). Embryo and brain antibody staining was performed as
264 described (Yang et al., 2019). Tissues were imaged with a Zeiss LSM800 confocal microscope. For
265 *Drosophila* eye imaging, *UAS-ORF3a/TM3, Sb* flies were crossed with *GMR-gal4* virgin flies to direct
266 expression of ORF3a in eyes. For wild type control, w^{1118} flies were crossed with *GMR-gal4* virgin flies.
267 Flies were crossed at 25°C for two days; the progeny were raised at 29°C, and female adults were
268 collected at day 3 post eclosure. Flies were frozen at −80°C for at least 24 h and imaged with a ZEISS
269 Axio Zoom V16 Microscope. Projected in-focus images were produced with the Montage Multifocus
270 module of the Zen Pro Software.

Cell culture

271 pCMV-GFP-SARS-CoV-ORF3a was generated by recombining the SARS-CoV-2-ORF3a coding
272 sequence (pDONR207 SARS-CoV-2 ORF3A, #141271, Addgene) into pDEST-CMV-N-EGFP (#122842,
273 Addgene). For LysoTracker staining, Hela cells were seeded in 6-well plates with cover slips and grown
274 to 50% confluency at 37°C with 5%CO2 in Dulbecco's modified Eagle's medium (12430047, Invitrogen)
275 supplemented with 10% heat-inactivated FBS (A4766801, Invitrogen). Cells were then transfected with
276 1000ng DNA, using standard Lipofectamine 3000 protocols (L3000008, Invitrogen). Media was changed
277 to DMEM with or without 10 μM chloroquine diphosphate (C6628, Sigma) 6h post transfection. 24h latter,
278 media was removed, and cells were incubated with 10 nM LysoTracker Red DND-99 (L7528, Invitrogen)
279 for 1h. Cells was washed with PBS for three times, mounted and imaged with a Zeiss LSM800 confocal
280 microscope.

Western blotting

281 For each sample, 10 adult female heads were homogenized in 200 μl IP buffer (20 mM Hepes, pH=7.4,
282 150 nM NaCl, 1% NP40, 1.5 mM MgCl2, 2 mM EGTA, 10 mM NaF, 1 mM Na3VO4, 1X proteinase
283 inhibitor), incubated on ice for 30 min and large debris was removed by 15min centrifugation (12,000Xg).
284 Anti-cleaved-caspase 3 (#9661, Cell Signaling Technology) and anti-beta-actin (E7-C, DSHB) were
285 used for immunoblotting. Western blots were performed by standard method using precast gels
286 (#456-1096, BioRad), and imaged with the ChemiDoc XRS+ system (BioRad).

Longevity and motor function assays

287 1d old adult flies were collected and transferred to fresh food daily for both assays. For longevity
288 analysis, the number of dead flies was recorded daily. Kaplan-Meier survival curves were generated,
289 and statistical analysis was performed using log-rank analysis (Prism9, GraphPad Software). To assess
290 motor function climbing assays were performed at described (Moore et al., 2018). Briefly, 15-20 flies
291 were placed into empty vials (9.5 cm high,1.7 cm in diameter) with flat bottoms, the flies were forced to
292 the bottom of a vial by firmly tapping the vial against the bench surface. Eight seconds after the tap, the
293 number of flies that climbed up the walls of a vial above the 5-cm mark was recorded as positive.

in vivo drug treatment

294 40mg/ml chloroquine phosphate (CQ, Sigma, C6628) was dissolved in water, and 40mg of CQ was
295 added to each 30g of fresh fly media. Adult flies were placed on treated food at 25°C for 2d and then
296 transferred. Progeny were cultured on CQ food from embryo stage to eclosion and transferred 24hr later
297 to normal media (to prevent adults from sticking to wet, treated media).

Quantitative real-time RT-PCR

298 Total RNA was extracted with TRIzol (15596026, Invitrogen), and quantitated with a Nanodrop 2000
299 (Thermo Fisher). cDNA was prepared by reverse transcription with All-in-One 5X RT MasterMix (G592,
300 Applied Biological Materials Inc) with 1000ng RNA. BlasTaq 2X qPCR MasterMix (G891, Applied
301 Biological Materials Inc) and ABI Step One system (Applied Biosystems) were used for quantitative
302 RT-PCR. Quantification was normalized to endogenous ribosomal protein Rp32 mRNA. RT-PCR
303 primers included:

304 Diptercin-F: GGCTTATCCGATGCCCGACG

305 Diptercin-R: TCTGTAGGTGTAGGTGCTTCCC

306 Attacin-A-F: ACGCCCGGAGTGAAGGATGTT

307 Attacin-A-R: GGGCGATGACCAGAGATTAGCAC

308 Drosomycin-F: GCAGATCAAGTACTTGTTCGCCC

309 Drosomycin-R: CTTCGCACCAGCACTTCAGACTGG

310 Eiger-F: AGCGGCGTATTGAGCTGGAG

311 Eiger-R: TCGTCGTCCGAGCTGTCAAC

Bioinformatic and statistical analysis

312 Protein alignments were generated by DNAMAN 10.0 (Lynnon Biosoft). All measurement data are
313 expressed as SEM. Comparisons of two samples were made using Student's t test, and multiple
314 samples by ANOVA. Survival curves were compared using the Kaplan–Meier test. P values of less than
315 0.05 were considered statistically significant. All statistical analyses were performed with GraphPad
316 Prism 9 software. The sample sizes and number of replicates are indicated in the figure legends. Data
317 collection and data analysis were routinely performed by different authors to prevent potential bias. All

318 individuals were included in data analysis.

Figure legends

319 **Figure 1. ORF3a is pathogenic in the nervous system**

320 **A.** ORF3a localization. *elav.Gal4* and *elav>ORF3a* adult brains labeled for ORF3a (green) and DAPI
321 (blue). ORF3a localized to cytoplasmic foci. **B.** Survival curves of *elav.Gal4* (control) and *elav>ORF3a*
322 adult flies. *elav>ORF3a* median lifespan was significantly less than controls. n>60 flies per genotype. **C.**
323 Longitudinal study of climbing ability. Locomotor activity was reduced in *elav>ORF3a* flies. Each data
324 point represents percent of flies that climbed above 5 cm, averaged for 3 independent trials. See Fig.
325 S1D. **D.** F_1 adult progeny from *elav.gal4,Sb/Tb* X *UAS-ORF3a/Sb* F_0 parents. 3 phenotypic classes with
326 an equivalent number of progeny (33.3%) were expected. *elav>ORF3a* flies were underrepresented. **E.**
327 Micrographs of 3d adult eyes. *GMR>ORF3a* eyes were rough and disorganized. **F.** Stage 16 embryonic
328 body wall muscles labeled with Tropomyosin. *Mef2>ORF3a* embryos showed largely normal body wall
329 musculature (see Fig. S1H for quantification). **G.** Apoptosis assay. *elav.Gal4* and *elav>ORF3a* adult
330 brains labeled for cleaved Caspase-3 (green) and DAPI (blue). ORF3a induced Caspase-3 cleavage. **H.**
331 Immunoblot of whole brain lysates from 3d *elav.Gal4* and *elav>ORF3a* adults validated results shown in
332 (**G**). **I.** qRT-PCR of RNA from 3d old adult heads. Transcripts encoding IMD pathway reporters (*dipt* and
333 *attA*) and a Toll pathway reporter (*Drs*) were enriched in *elav>ORF3a* flies. n>20 unless otherwise noted.
334 Error bars represent standard error of the mean (SEM) from at least three independent replicates.
335 Significance was determined by log-rank test (B), two-way ANOVA (C), and student's t-test (I). *$p < 0.05$,
336 **$p < 0.01$, ****$p < 0.0001$, (ns) non-significant.

337 **Figure S1. Related to Figure 1.**

338 **A.** Protein alignment of SARS-Cov-ORF3a and SARS-Cov-2-ORF3a. Dark blue shading shows identical
339 residues, light blue shading shows similar residues. **B.** PCR of genomic DNA from ORF3a two
340 independent transgenic lines. ORF3a band is indicated with red arrow. **C.** RT-PCR of *ORF3a* mRNA
341 shows *ORF3a* expression is induced in muscle (*Mef2.Gal4*) and in the nervous system (*GMR.Gal4*).
342 ORF3a band is shown (red arrow). **D.** Representative result of a climbing assay. *elav>ORF3a* flies (right)
343 had reduced motor function. **E.** 6d old female flies. *elav>ORF3a* flies (right) showed severely swollen
344 abdomens. **F.** Survival curves of *Mef2.Gal4* (control) and *Mef2>ORF3a* adult flies. *Mef2>ORF3a* median

345 lifespan was not significantly different than controls. n>60 flies per genotype. **G.** Longitudinal study of
346 climbing ability. Locomotor activity was unaffected in *Mef2>ORF3a* flies. Each data point represents
347 percent of flies that climbed above 5 cm, averaged for 3 independent trials. **H.** Quantification of
348 embryonic body wall muscle phenotypes from Fig. 1F. Diagram shows the 30 muscles per embryonic
349 segment; blue muscles were 100% normal in >60 *Mef2>ORF3a* embryonic segments, red muscles
350 showed a developmental phenotype in at least 1 of the 60 segments. Dot plot shows frequency of
351 muscle phenotypes is <9.0%. (ns) not significant.

352 **Figure 2. Chloroquine (CQ) protects against ORF3a-induced dysfunction.**

353 **A.** Survival curves of *elav.Gal4* (control), *elav>ORF3a*, and CQ treated *elav>ORF3a* adult flies. CQ
354 treatment significantly extended *elav>ORF3a* median lifespan. n>60 flies per genotype **B.** Longitudinal
355 study of climbing ability. Locomotor activity was significantly improved in *elav>ORF3a* flies treated with
356 CQ. Each data point represents percent of flies that climbed above 5 cm, averaged for 3 independent
357 trials. **C.** F_1 adult progeny treated with CQ from *elav.gal4,Sb/Tb* X *UAS-ORF3a/Sb* F_0 parents. 3
358 phenotypic classes with an equivalent number of progeny (33.3%) were expected. CQ treatment
359 improved *elav>ORF3a* survivability to adulthood (compare to Fig. 1D). **D.** Immunoblot of whole brain
360 lysates from 3d *elav.Gal4, elav>ORF3a,* and CQ treated *elav>ORF3a* adults. CQ reduced cleaved
361 Caspase-3 levels in *elav>ORF3a* flies. **E,F.** qRT-PCR of RNA from 3d old adult heads. CQ treatment
362 blunted the expression of the Toll pathway reporter *Drs* (E), but not IMD pathway reporters (*dipt* and *attA*;
363 F) in *elav>ORF3a* flies. **G.** Live imaging of HELA cells transfected with CMV-GFP-ORF3a (green) for
364 24hr, treated with or without CQ, and labeled with Lysotracker (red). ORF3a transfected cells showed
365 reduced Lysotracker staining (deacidified lysosomes) than untransfected controls (outlined in heat map).
366 CQ treatment restored Lysotracker staining in ORF3a expressing cells **(H)**. n>20 unless otherwise noted.
367 Error bars represent standard error of the mean (SEM) from at least three independent replicates.
368 Significance was determined by log-rank test (A), two-way ANOVA (B), and student's t-test (H). *$p < 0.05$,
369 **$p < 0.01$, ****$p < 0.0001$, (ns) non-significant.

Figure 1 ORF3a is pathogenic in nervous system

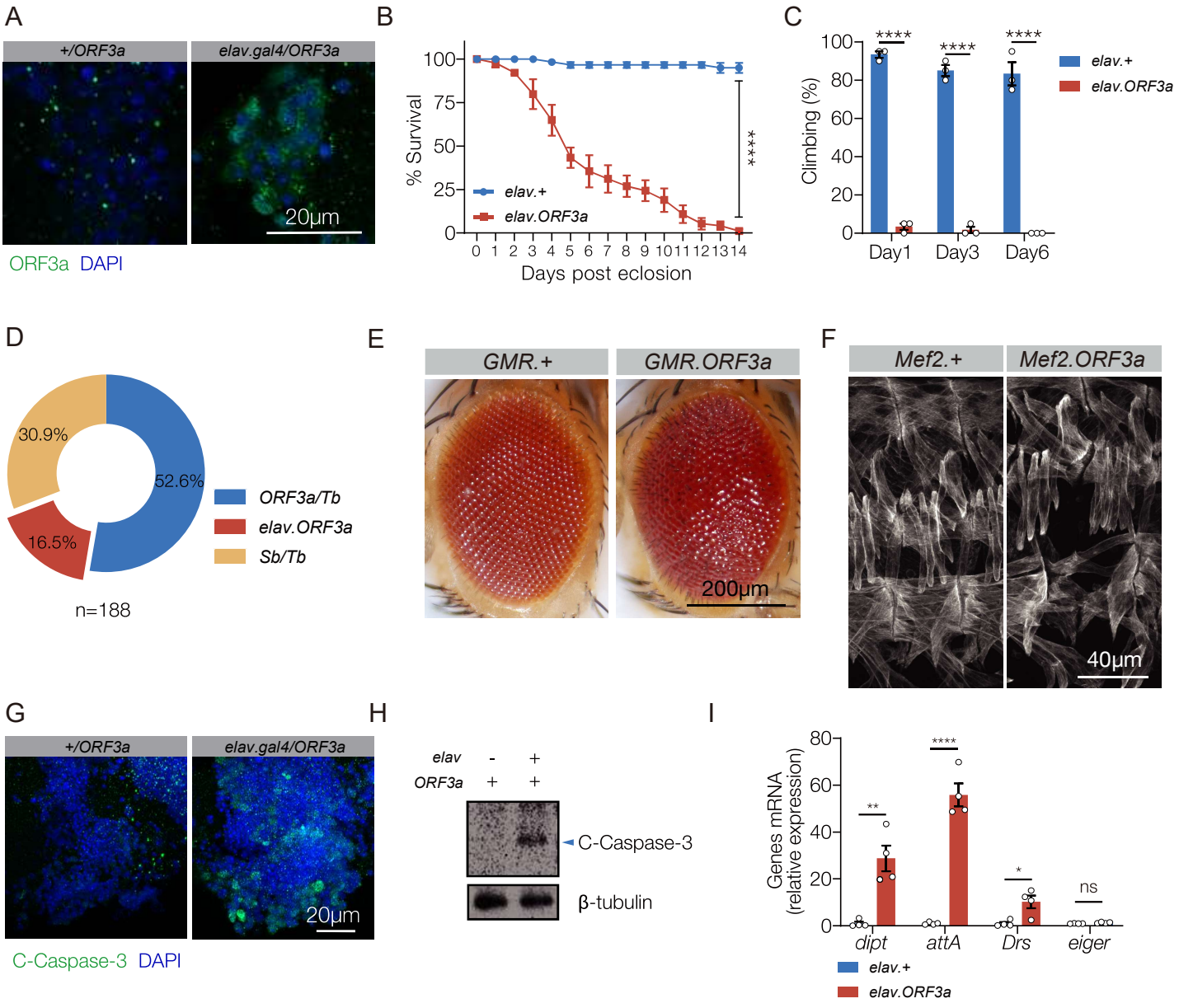

Supplemental Figure 1, related to Figure 1

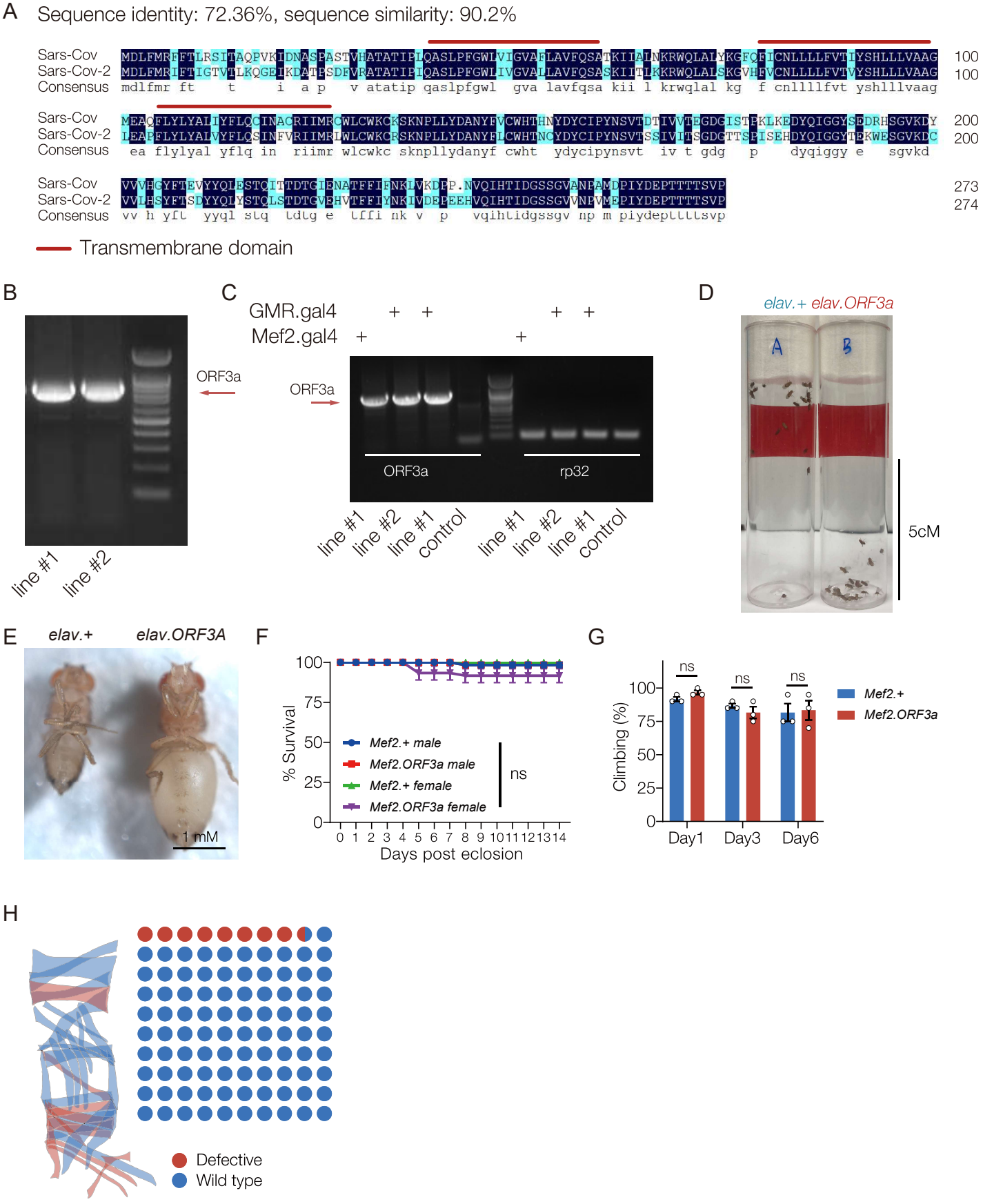
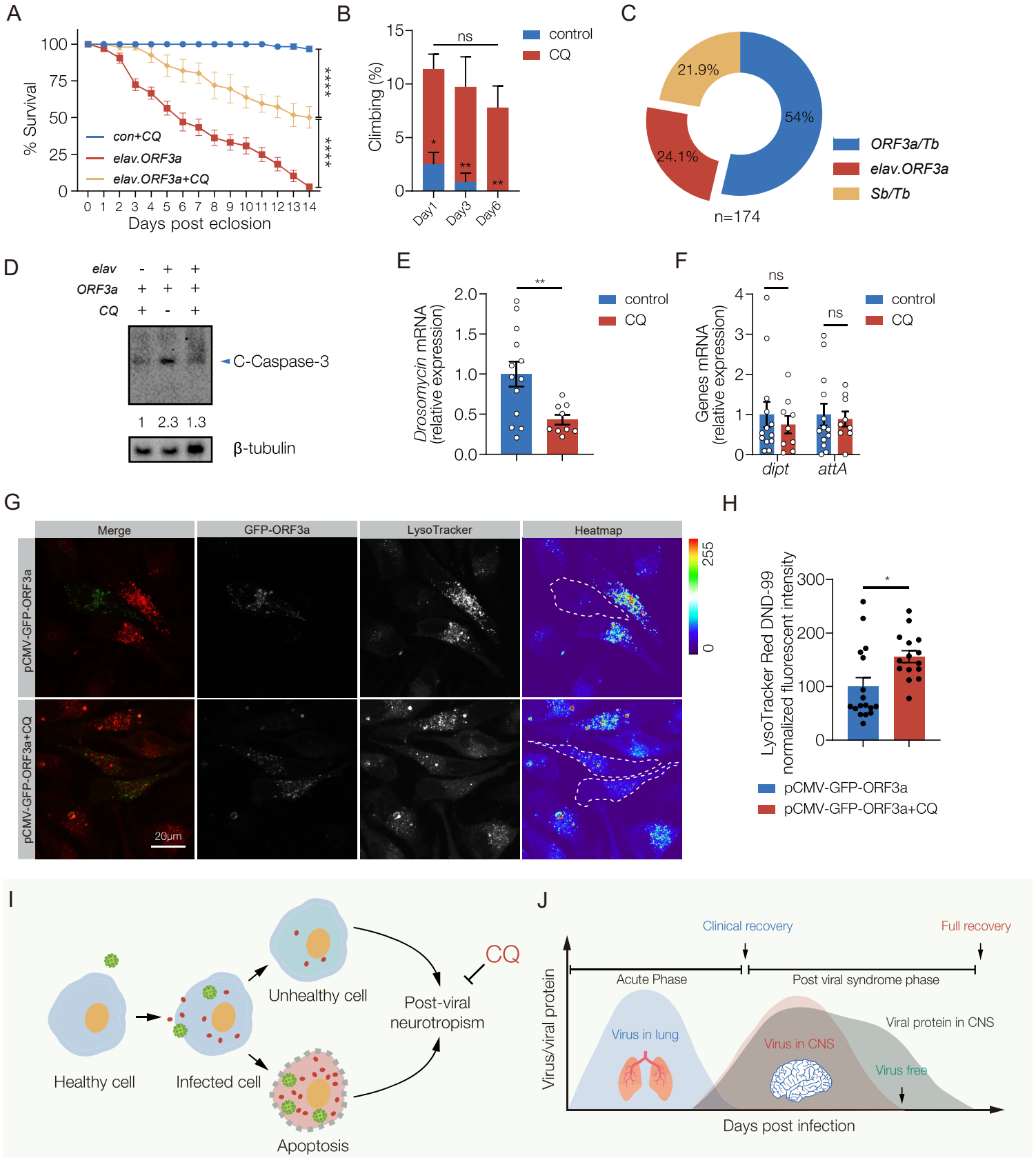
Figure 2 Chloroquine protects against ORF3a induced dysfunction